

## Supporting Information

### **Stretchable, conductive and porous MXene-based multilevel structured fibers for sensitive strain sensing and beyond**

Qing Guo, Weiwei Pang, Xia Xie, Yanling Xu, Wenjing Yuan\*

School of Materials Science & Engineering, Tianjin Key Laboratory of Materials Laminating Fabrication and Interface Control Technology, Hebei University of Technology, Tianjin 300130, China.

\*Corresponding authors: ywj11@tsinghua.org.cn;

## Supplementary Methods

### 1.1 Preparation of MXene

MXene was prepared according to the previous literatures<sup>1, 2</sup>. In brief, a total of 0.5 g of  $\text{Ti}_3\text{AlC}_2$  MAX powders were gradually added (in the course of 5 min) into the etching solution containing LiF and HCl (9 M HCl, 0.8 g LiF) under stirring. The etching reaction was allowed to proceed at 35 °C for 24 h. Then, the reaction mixture was washed with deionized water via centrifugation (10 min per cycle at 10000 rpm) for 6–8 times until the pH of the supernatant was close to 6. During this washing process, the sediment was observed to be swollen due to water intercalation. The dark green sediments were collected and redispersed into an additional 50 mL of deionized water, followed by delamination under sonication (100 W) for 10 min. The obtained  $\text{Ti}_3\text{C}_2\text{T}_x$  dispersion was further centrifuged at 3500 rpm for 20 min to remove the unexfoliated MAX, and the top 80% supernatant was decanted for further use. The concentration of the final MXene dispersion was measured to be 8–10 mg mL<sup>-1</sup>.

### 1.2 Gas sensing test

The gas sensing performance of the fiber was measured in a gas sensing testing system. Silver wires were glued to each end of the fiber with silver paste and connected with the electrodes of the analyzer. The fiber sensor was placed in a quartz chamber with a gas inlet and outlet. A constant voltage of 1V was applied onto the fiber, and the current variation was recorded with an electrochemical analyzer (CHI 660E). The sensing chamber was first purged with  $\text{N}_2$  (99.99%) to evacuate the air. After a stable baseline current was obtained, target gas (acetone, ethanol, methanol,  $\text{NH}_3$ ,  $\text{SO}_2$ ,  $\text{O}_2$ ,  $\text{CO}_2$ , or  $\text{H}_2\text{O}$  balanced in  $\text{N}_2$ ) and purging gas were introduced into the chamber alternatively. The concentration of the gas was controlled through altering the flow rates of the target gas and balanced gas with mass flow controllers. The total flow rate was fixed at 500 sccm. The temperature was controlled to be  $25 \pm 2$  °C.

## 2. Supplementary Figures

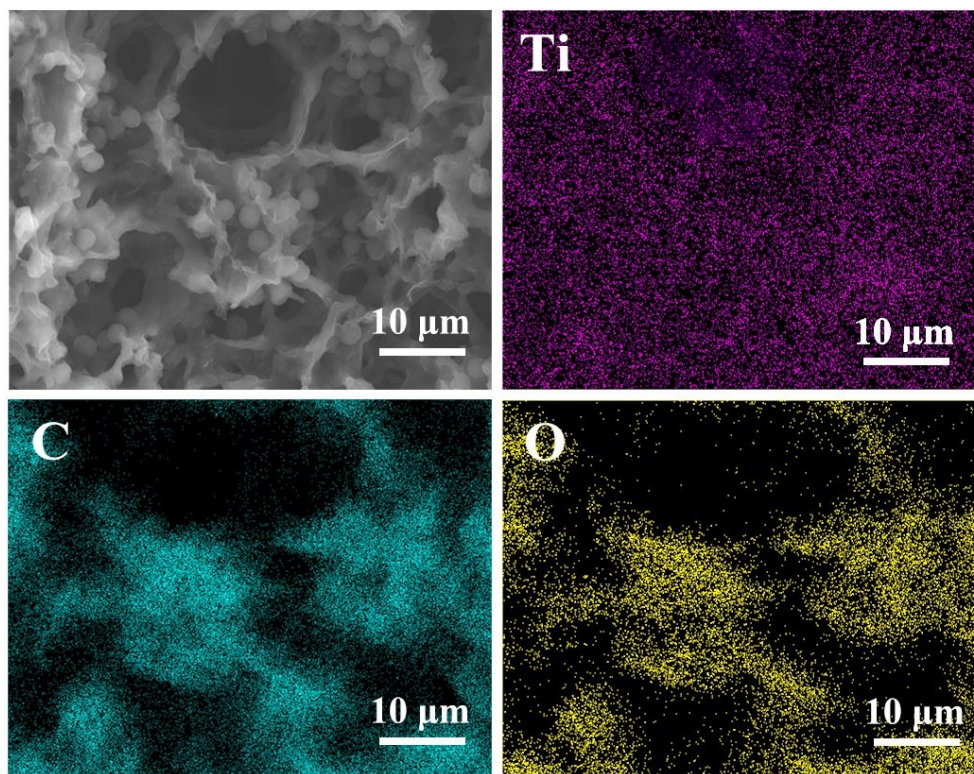


**Fig. S1** (a) SEM image showing the porous fiber core and (b-d) the corresponding elemental mapping of Ti, C and O, indicating uniform distribution of the MXene@spheres.

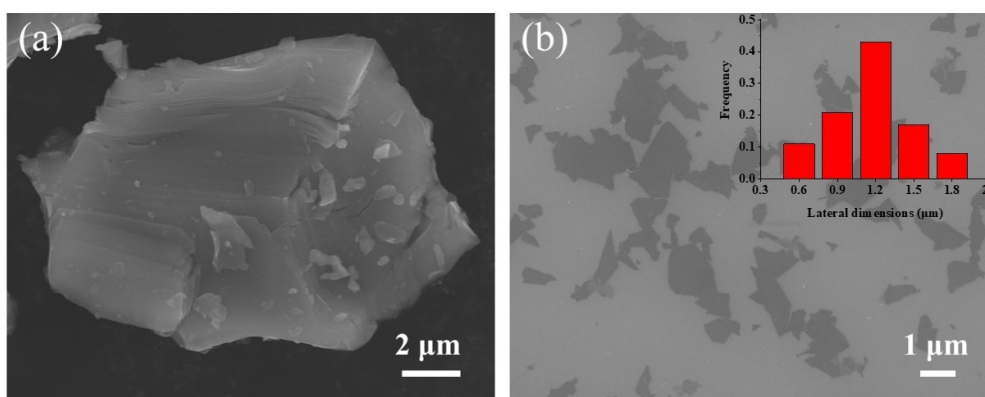


**Fig. S2** SEM images of bulk MAX (a) and corresponding MXene sheets (b). The average lateral dimension of the sheets was 1.2 μm.

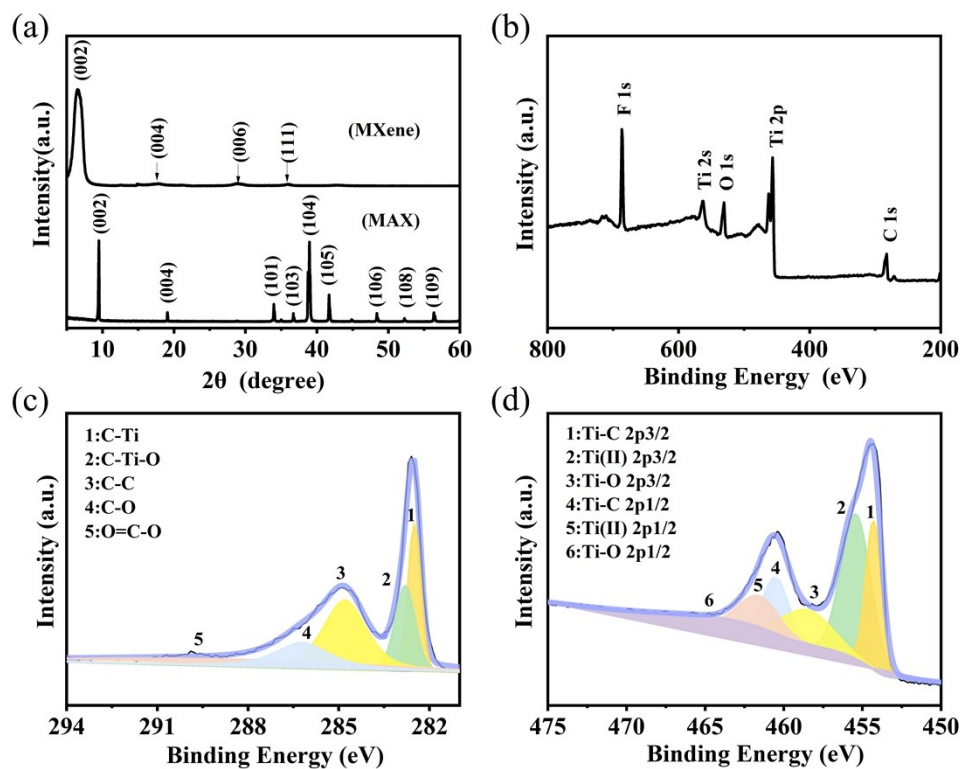


**Fig. S3** Chemical structure characterization of MXene. **(a)** XRD patterns of  $Ti_3C_2T_x$  MXene and corresponding MAX. The (002) peak shifted towards lower angles and the (104) peak attributed to the MAX phase disappeared, suggesting the successful etching of Al layers and the formation of MXene phase. **(b-d)** XPS full spectrum **(b)**, high-resolution C1s **(c)** and Ti 2p **(d)** spectra showing the chemical structure and bonding configuration of MXene.

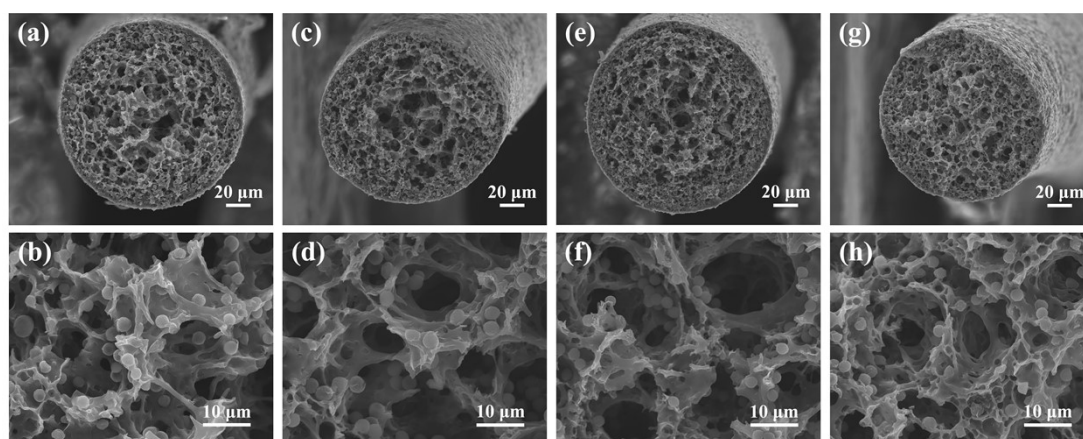


**Fig. S4** SEM images of the porous MXene@sphere fibers with different MXene loading: **(a, b)** 4%, **(c, d)** 5%, **(e, f)** 6%, **(g, h)** 7%.

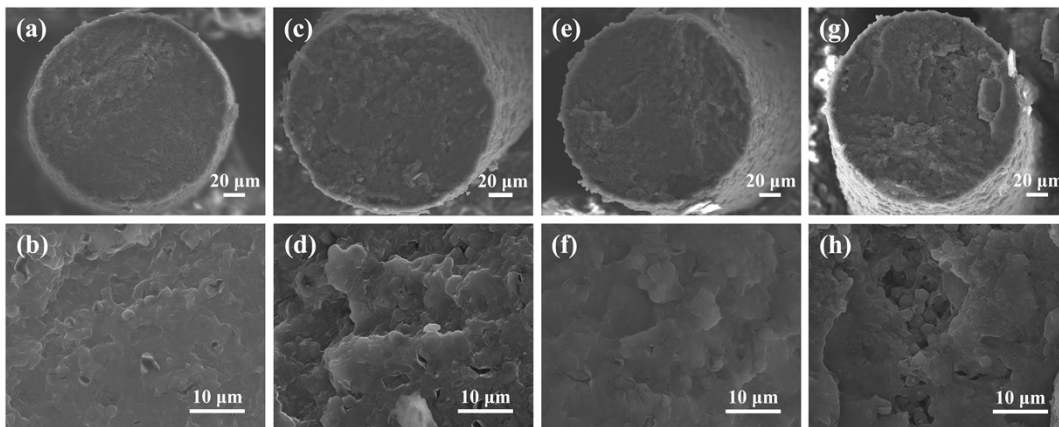


**Fig. S5** SEM images of the solid MXene@sphere fibers with different MXene loading: (a, b) 4%, (c, d) 5%, (e, f) 6%, (g, h) 7%.

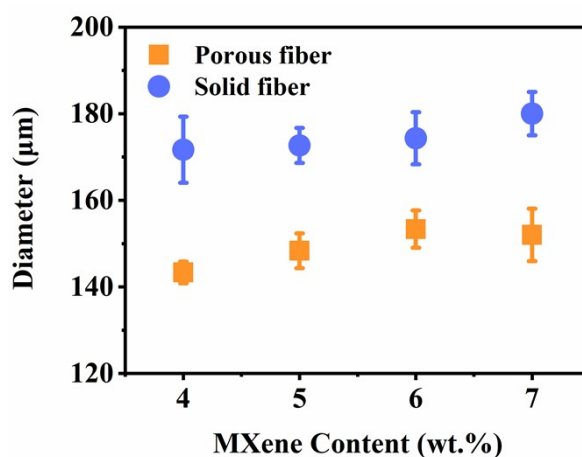


**Fig. S6** Diameters of the MXene@sphere fibers produced using IPA or AA at various MXene loadings.

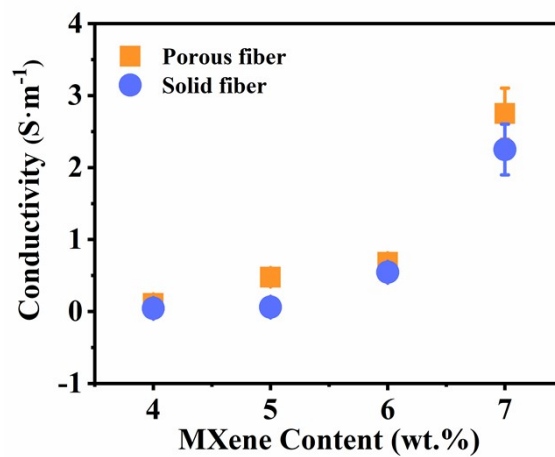


**Fig. S7** Conductivity of the wet-spun fibers with various MXene content.

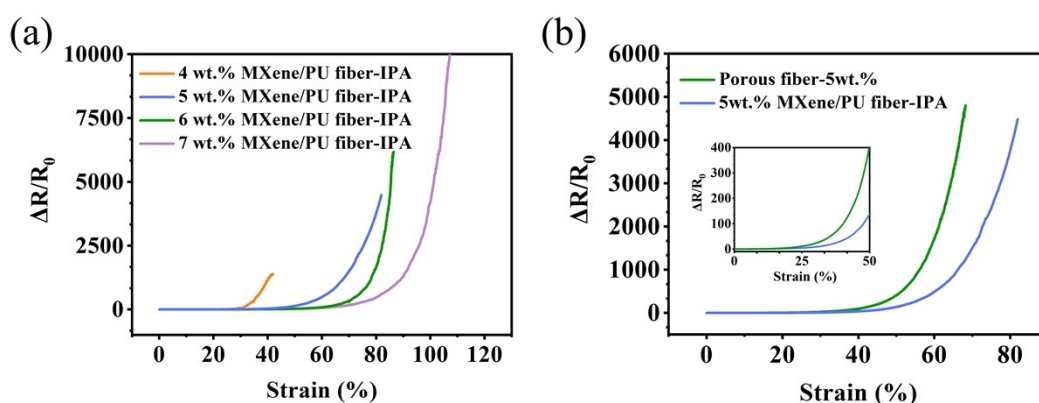


**Fig. S8** (a) Strain sensing responses of the MXene/PU fibers without PS spheres. (b) Comparison of strain sensing behaviors between porous fiber with PS spheres and MXene/PU fiber without PS spheres at 5 wt.% MXene loading.

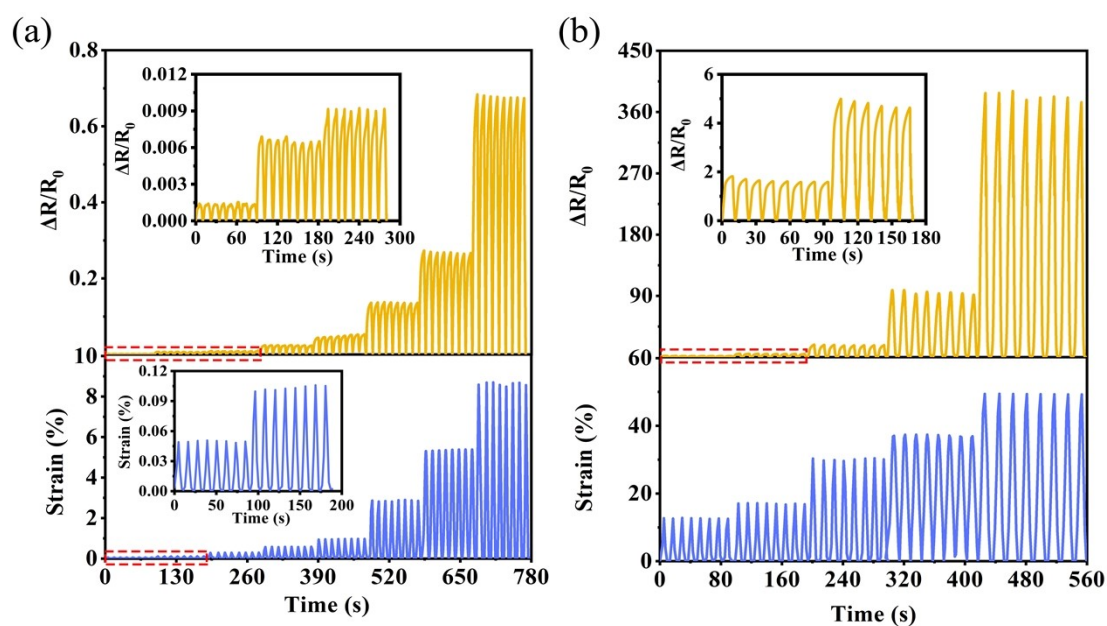


**Fig. S9** Strain sensing performance of the porous MXene@sphere fiber. (a, b) Cyclic strain sensing responses of the porous fiber at tensile strain of 0.05-9% (a), and 13-50% (b).

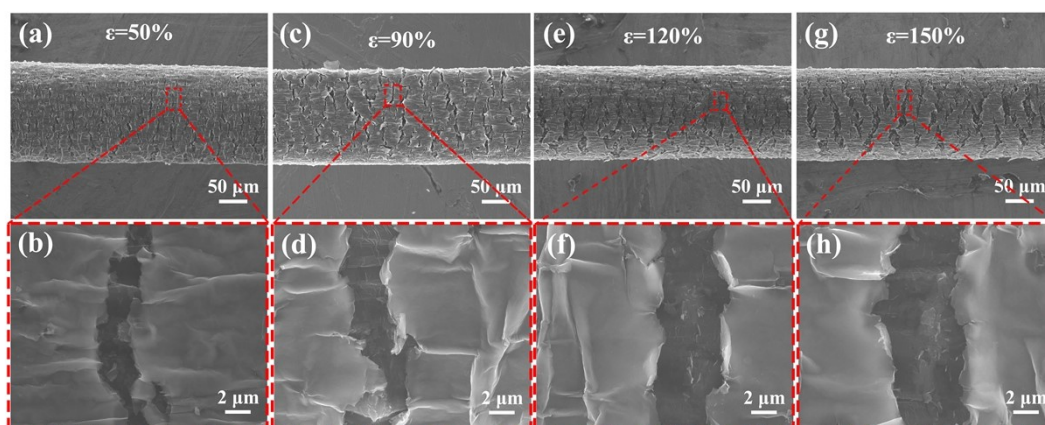


**Fig. S10** Morphology of the multilevel structured fiber under different tensile strains.

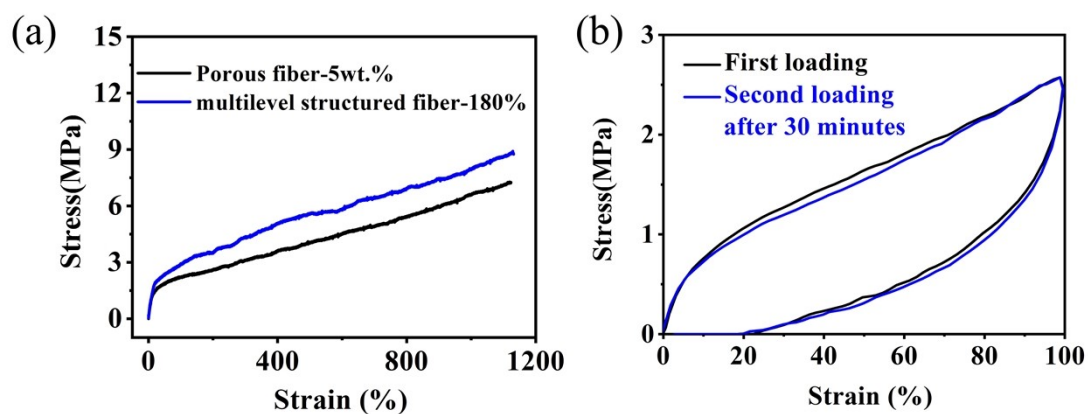


**Fig. S11** (a) Comparison of the stress-strain curves of the multilevel structured fiber and the porous fiber core. (b) Cyclic stress-strain curves of the multilevel structured fiber with first loading (black) and second loading (blue) after 30 min rest. At a stretching rate of  $100\% \text{ min}^{-1}$ .

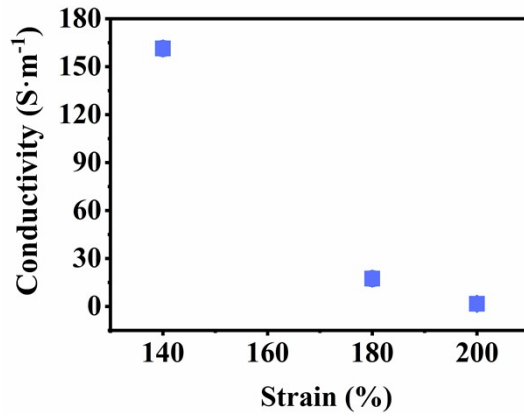


**Fig. S12** Conductivity of the multilevel structured fiber with various second guide strain.

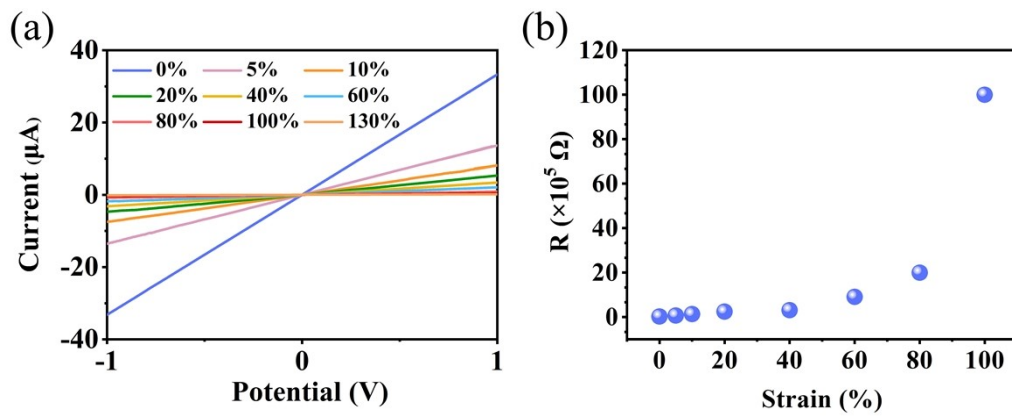


**Fig. S13** (a) Strian sensing responses of the multilevel structured fiber under static strain loadings. (b) Resistance value under different strains extracted from (a).

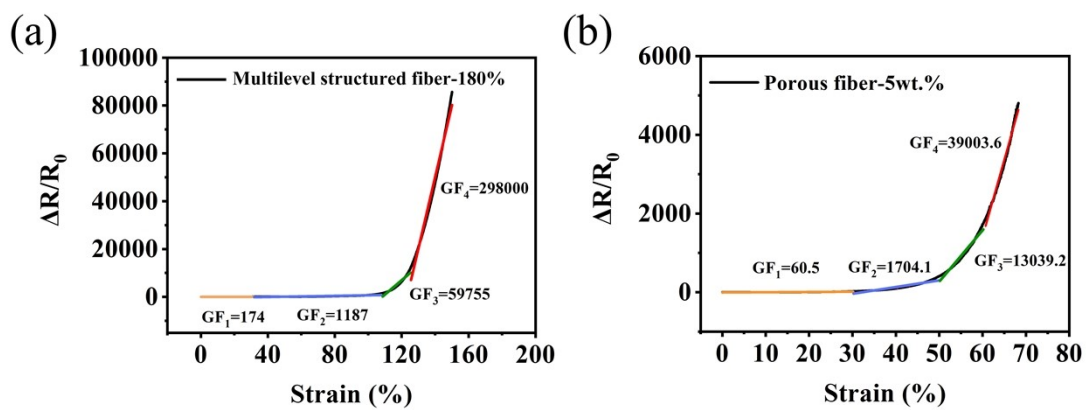


**Fig. S14** Sensitivity over different strain ranges extracted from the sensing plot. (a) Multilevel structured fiber with 180% second guide strain. (b) Porous fiber core.

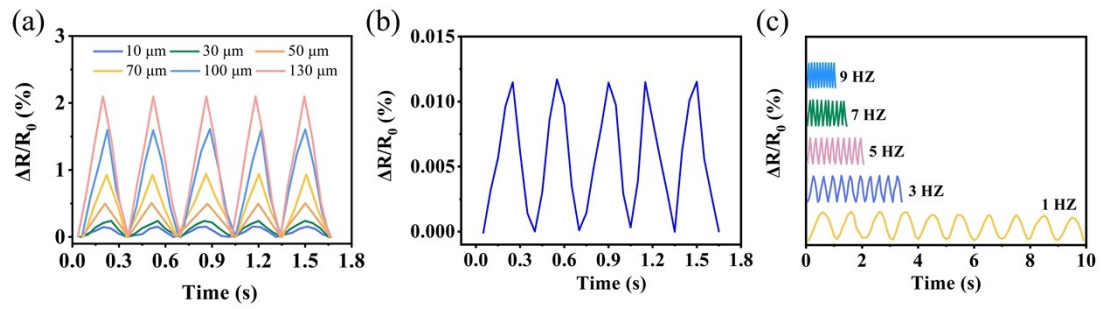


**Fig. S15** Strain sensing performance of the multilevel structured fiber under sinusoidal vibrations. **(a)** Sensing responses under various vibrating amplitudes with a frequency 3 Hz. **(b)** Sensing responses under vibrating amplitude of 5  $\mu\text{m}$ . **(c)** Sensing response under various vibrating frequency with an amplitude of 20  $\mu\text{m}$ .

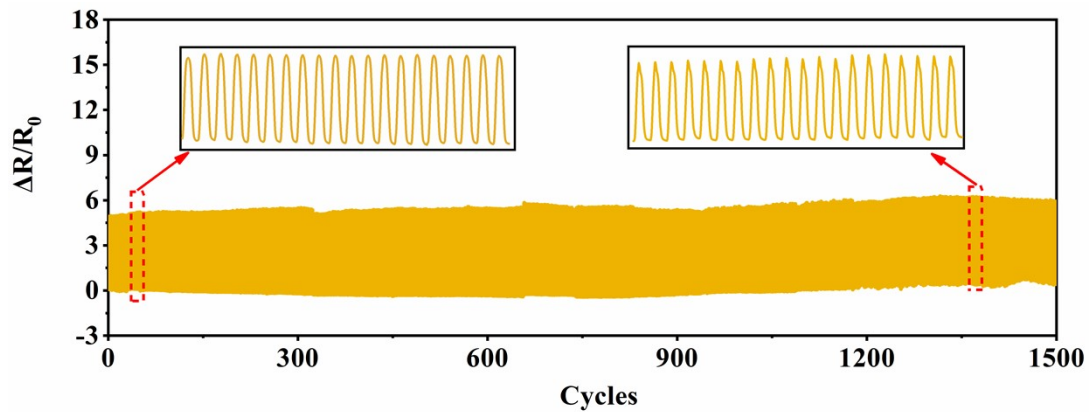


**Fig. S16** Sensing stability of the multilevel structured fiber over 1500 cycles of stretching and releasing.

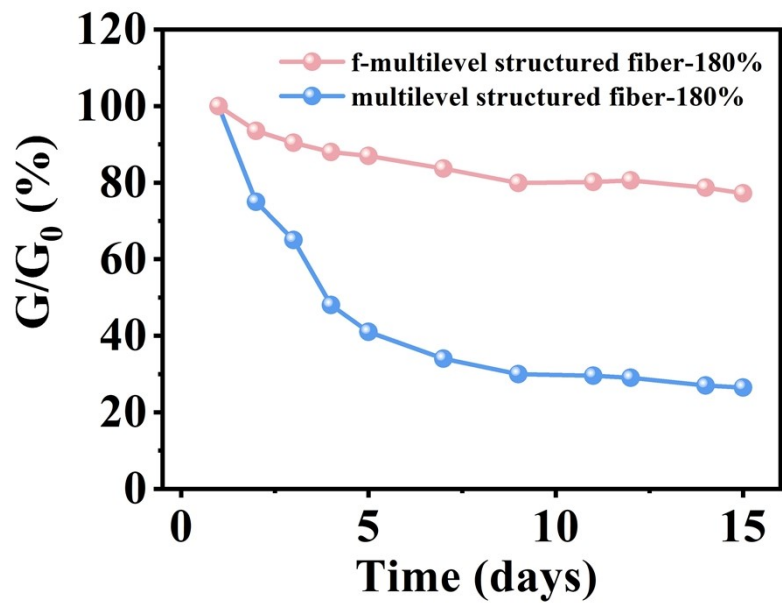


**Fig. S17** Conductivity stability of the fibers stored in ambient environment over 15 days.

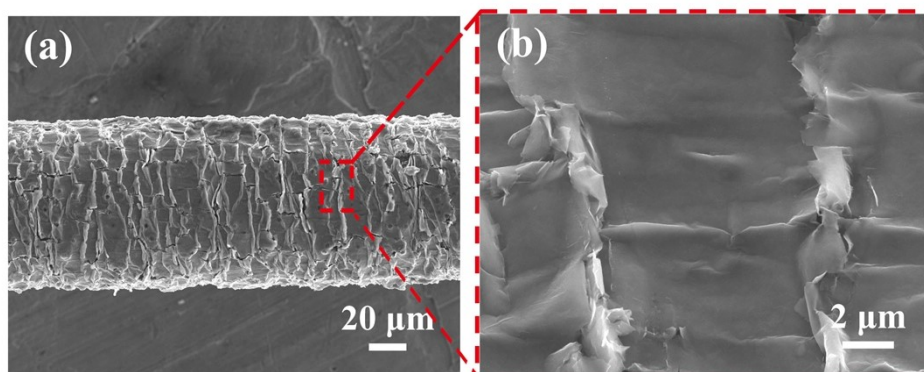


**Fig. S18** Morphology of the multilevel structured fiber after stretching/releasing for hundreds of cycles.

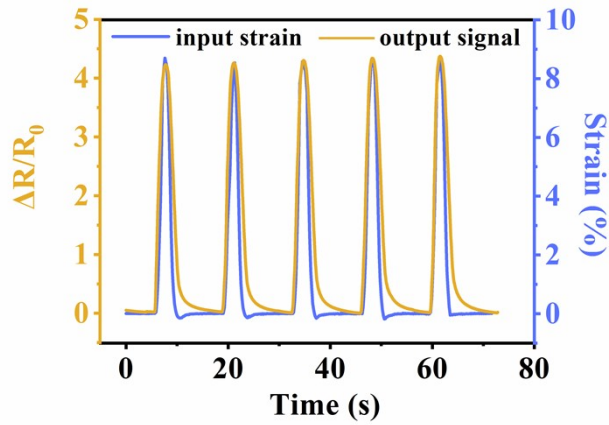


**Fig. S19** Sensing response of the multilevel structure fiber with the output resistance signal well overlapping with the input strain signal.

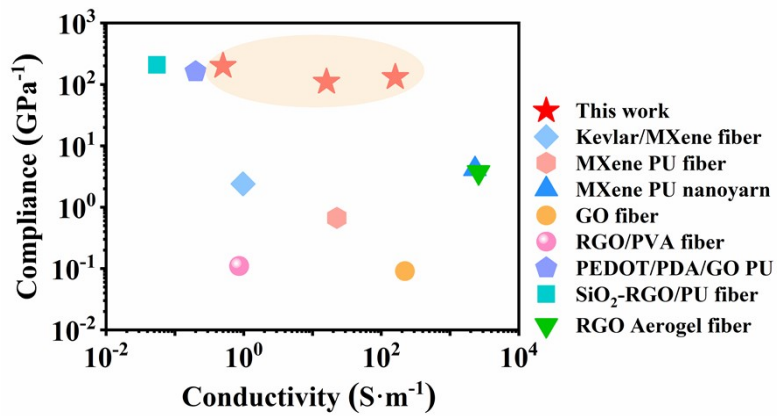


**Fig. S20** Comparison of compliance and conductivity of the multilevel structured fiber with composite fibers reported in the literatures.<sup>3-10</sup>

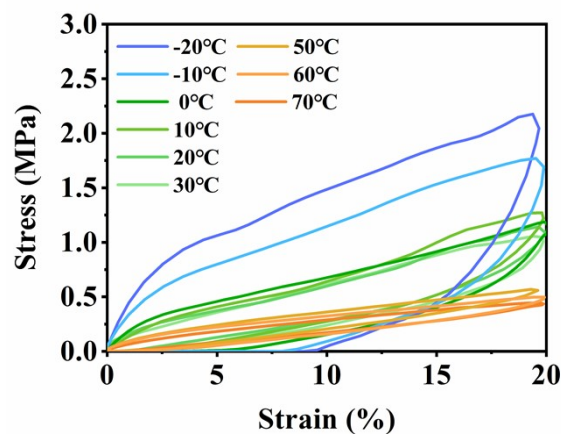


**Fig. S21** Stress-strain curves of the multilevel structured fiber under different

temperatures.

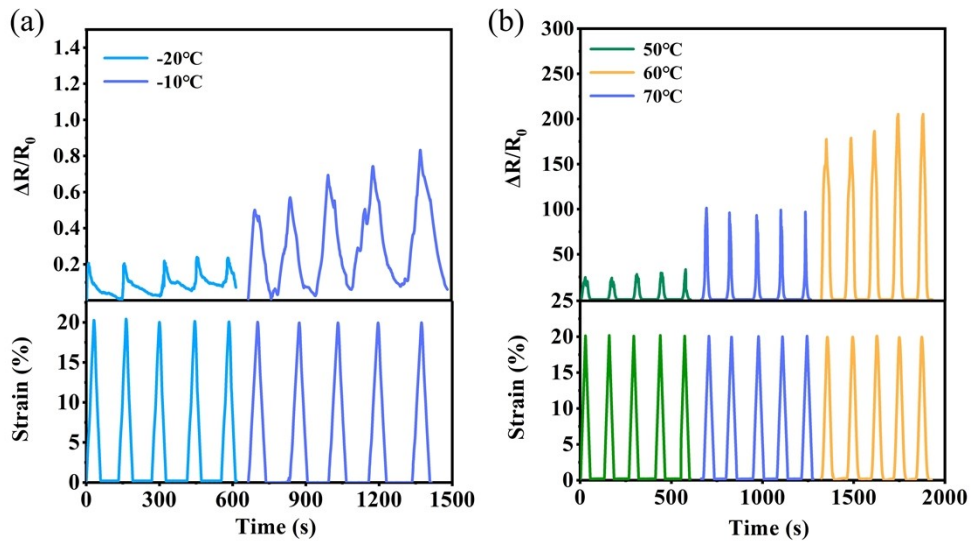


**Fig. S22** Strain sensing behavior of the multilevel structured fiber at temperatures lower than 0 °C (a), and higher than 30 °C (b).

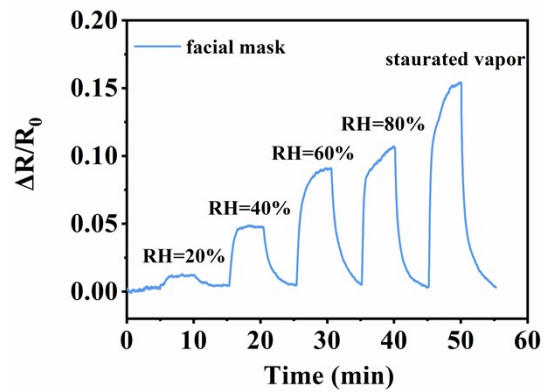


**Fig. S23** Humidity sensing response of the integrated fiber sensor.

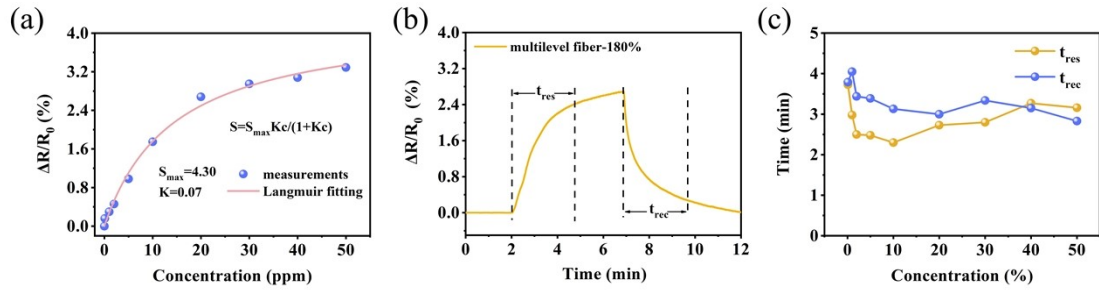


**Fig. S24** Gas sensing performance analysis. (a) Response intensity versus acetone concentration plot and the corresponding Langmuir fitting curve. (b) Response and recovery time of the sensing response. (c) Response and recovery times of the sensor under different acetone concentrations.

**Table S1.** Comparison of the sensing performance of the multilevel structured fiber with those reported in previous literatures.

Materials	Method	Stretchable or flexible	Response	LOD (ppm)	Sensing range (ppm)	Response/recover time (min)	Sensitive targets	Ref
Multilevel structured fiber	Wet-spinning	Stretchable (~1000%)	1.77% (10 ppm)	0.1	0.1-50	2.3/3.13	Acetone, Ethanol, NO <sub>2</sub>	This work
Ti <sub>3</sub> C <sub>2</sub> T <sub>x</sub> MXene	Filtration	—	1.18% (100 ppm)	0.05-0.1	0.05-1000	—	Acetone, Ethanol, Ammonia	11
MXene/PU fiber-5%	Wet-spinning	Stretchable (>400%)	1.2% (10 ppm)	0.05	0.05- Saturated vapor	3.5/3.5	Acetone, Ethanol, Methanol	12
Ti <sub>3</sub> C <sub>2</sub> T <sub>x</sub> MXene	Depositing	Flexible	1.72% (100 ppm)	100	100-800	0.98/1.18	Acetone, Ethanol, Methanol	13
Ti <sub>3</sub> C <sub>2</sub> T <sub>x</sub> -F MXene	Spray-coating	Flexible	3.5% (30 ppm)	5	5-120	2/2.33	Ethanol, Acetone, 2-propanol	14
3@SWCNT on paper	Filtered & Dried under vacuum	Flexible	3.9% (20 ppm)	20	20-500	0.61/1.41	Acetone, Ethanol, Methanol	15
La(TBPP) (TBNc)	Solution & Vapor annealing	Flexible	57% (100 ppm)	0.2	0.2-800	1.25/1.48	Acetone	16
SWNTs-poly(TPP)	LPCVD	Flexible	<0.5% (50 ppm)	9	50-230000	8/—	Acetone	17
SnO <sub>2</sub> -RGO composite film	Hydrothermal method	Flexible	2.19% (10 ppm)	10	10-2000	1.78/1.58	Acetone	18
MXene/rGO/CuO aerogel	Freeze-drying	Flexible	52% (100 ppm)	10	10-500	0.1/0.125	Acetone, Trimethyl	19

MXene-PI	solution deposition	Flexible	0.034% (25 ppm)	25	25-200	5/5	amine, Triethylamine, Acetone, Ethanol, Methanol	20
Ti <sub>3</sub> C <sub>2</sub> T <sub>x</sub> /γ-PGA	Spraying	Flexible	100% (10 ppm)	2	2-50	0.72/0.05	NO <sub>2</sub>	21
Nb <sub>2</sub> CT <sub>x</sub> /SA composite films	Electrospinning	Flexible	5.3V (91.5%RH)	18.7% RH	0-91.5% RH	0.45/0.34	Humidity	22
Alkalized V <sub>2</sub> CT <sub>x</sub> MXene	Drop-casting	Flexable	19.9% (20 ppm)	5	5-50	1.27/0.33	NO <sub>2</sub>	23
PANI/Nb <sub>2</sub> CT <sub>x</sub>	Spraying	Flexible	74.68 % (10 ppm)	0.02	0.02-50	3.6/5	NH <sub>3</sub>	24

### 3. Supplementary References

1. M. Alhabeab, K. Maleski, B. Anasori, P. Lelyukh, L. Clark, S. Sin and Y. Gogotsi, *Chem. Mater.*, 2017, **29**, 7633-7644.
2. C. Zhang, L. McKeon, M. P. Kremer, S.-H. Park, O. Ronan, A. Seral-Ascaso, S. Barwich, C. O. Coileain, N. McEvoy, H. C. Nerl, B. Anasori, J. N. Coleman, Y. Gogotsi and V. Nicolosi, *Nat. Commun.*, 2019, **10**, 1795.
3. B. Cheng and P. Wu, *ACS Nano*, 2021, **15**, 8676-8685.
4. Z. Xu, Y. Zhang, P. Li and C. Gao, *ACS Nano*, 2012, **6**, 7103-7113.
5. R. Jalili, S. H. Aboutaleb, D. Esrafilzadeh, R. L. Shepherd, J. Chen, S. Aminorroaya-Yamini, K. Konstantinov, A. I. Minett, J. M. Razal and G. G. Wallace, *Adv. Funct. Mater.*, 2013, **23**, 5345-5354.
6. S. Seyedin, S. Uzun, A. Levitt, B. Anasori, G. Dion, Y. Gogotsi and J. M. Razal, *Adv. Funct. Mater.*, 2020, **30**, 1910504.
7. J. Gao, B. Li, X. Huang, L. Wang, L. Lin, H. Wang and H. Xue, *Chem. Eng. J.*, 2019, **373**, 298-306.
8. B. Li, J. Luo, X. Huang, L. Lin, L. Wang, M. Hu, L. Tang, H. Xue, J. Gao and Y.-W. Mai, *Compos. B. Eng.*, 2020, **181**, 107580.
9. X. Fu, L. Li, S. Chen, H. Xu, J. Li, V. Shulga and W. Han, *J. Colloid Interface Sci.*, 2021, **604**, 643-649.
10. L. Kou and C. Gao, *Nanoscale*, 2013, **5**, 4370-4378.
11. S. J. Kim, H. J. Koh, C. E. Ren, O. Kwon, K. Maleski, S. Y. Cho, B. Anasori, C. K. Kim, Y. K. Choi, J. Kim, Y. Gogotsi and H. T. Jung, *Acs Nano*, 2018, **12**, 986-993.
12. Y. Tang, Y. Xu, J. Yang, Y. Song, F. Yin and W. Yuan, *Sensors and Actuators B: Chemical*, 2021, **346**, 130500.
13. D. Li, G. Liu, Q. Zhang, M. Qu, Y. Q. Fu, Q. Liu and J. Xie, *Sensors and Actuators B: Chemical*, 2021, **331**, 129414.
14. W. Y. Chen, S. N. Lai, C. C. Yen, X. Jiang, D. Peroulis and L. A. Stanciu, *Acs Nano*, 2020, **14**,

- 11490-11501.
15. E. Baysak, S. Yuvayapan, A. Aydogan and G. Hizal, *Sensors and Actuators B: Chemical*, 2018, **258**, 484-491.
  16. P. Zhu, S. Li, X. Jiang, Q. Wang, F. Fan, M. Yan, Y. Zhang, P. Zhao and J. Yu, *Anal Chem*, 2019, **91**, 10320-10327.
  17. T. Sarkar, S. Srinives, S. Sarkar, R. C. Haddon and A. Mulchandani, *The Journal of Physical Chemistry C*, 2014, **118**, 1602-1610.
  18. D. Zhang, A. Liu, H. Chang and B. Xia, *RSC Advances*, 2015, **5**, 3016-3022.
  19. M. Liu, Z. Wang, P. Song, Z. Yang and Q. Wang, *Sensors and Actuators B: Chemical*, 2021, **340**, 129946.
  20. E. Lee, A. VahidMohammadi, B. C. Prorok, Y. S. Yoon, M. Beidaghi and D. J. Kim, *ACS Appl Mater Interfaces*, 2017, **9**, 37184-37190.
  21. Q. Zhao, D. Sun, S. Wang, Z. Duan, Z. Yuan, G. Wei, J. L. Xu, H. Tai and Y. Jiang, *ACS Sens*, 2021, **6**, 2858-2867.
  22. Q. Zhao, Y. Jiang, Z. Duan, Z. Yuan, J. Zha, Z. Wu, Q. Huang, Z. Zhou, H. Li, F. He, Y. Su, C. Tan and H. Tai, *Chem Eng J*, 2022, **438**, 135588.
  23. Y. Zhang, Y. Jiang, Z. Duan, Q. Huang, Y. Wu, B. Liu, Q. Zhao, S. Wang, Z. Yuan and H. Tai, *Sensors and Actuators B: Chemical*, 2021, **344**, 130150.
  24. S. Wang, Y. Jiang, B. Liu, Z. Duan, H. Pan, Z. Yuan, G. Xie, J. Wang, Z. Fang and H. Tai, *Sensors and Actuators B: Chemical*, 2021, **343**, 130069.